

Modeling and simulation of a dual temperature BTES system

Mohammadamin Ahmadfard¹, Michel Bernier¹, Antoni Paleshi², Greg Allen³

¹Polytechnique Montréal, Montréal, Canada

²WSP, Kitchener, Ontario, Canada

³Rivercourt Engineering, Toronto, Canada

Abstract

The concept of a dual temperature borehole thermal energy storage (DT-BTES) system is presented in this paper. DT-BTES consists of relatively warm boreholes positioned in an inner core and surrounded by colder boreholes on an outer ring. The differential temperature between these two sets of boreholes can be achieved using a heat pump that uses the outer ring as the source and the inner core as a sink.

In the first part of the paper, the approach used to model borehole heat transfer in a DT-BTES is presented. Then, the DT-BTES model is used in two multi-annual simulation test cases. In the second test case, heat pumps operate overnight so that the inner core and the outer ring are sufficiently hot and cold for direct heating and cooling of a building during the daytime. These results show the potential of DT-BTES systems to displace electrical energy usage.

Introduction

Borehole thermal energy storage (BTES) systems are categorized based on their temperature range, size, configuration, and applications. Gehlin (2016) has comprehensively reviewed BTES systems and noted no uniform definition for BTES systems. However, it is generally agreed that some form of intentional thermal storage in the ground for long periods is required to be qualified as a BTES. Low-temperature BTES systems (with storage temperatures near the undisturbed ground temperature) have a more significant potential to be used globally than high-temperature BTES systems due to their relatively high storage efficiencies.

Low-temperature BTES systems are most efficient for space heating and cooling buildings with fairly balanced loads (Gehlin, 2016). For these systems, it is suggested to maintain the average storage temperature close to the annual ambient average temperature, which typically corresponds to the undisturbed ground temperature (Chapuis and Bernier 2008, 2009). This helps limit the heat losses from the BTES and avoid exceeding the operational temperature limit of the heat pumps, but on her hand, it reduces the efficiency of the solar collectors connected to the core (Eslami-nejad et al., 2009).

To reduce the peak electricity need of a residential building in Toronto, Teamah and Lightstone (2019) used borehole thermal storage coupled with a buffer tank. The buffer tank contains water or a mix of water and phase change materials (PCMs) to store sensible and latent energy. Results showed that this configuration reduces greenhouse gas (GHG)

emissions during peak electricity demand periods when natural gas power plants are employed. It also helps the consumers benefit from significantly reduced energy rates if utilities employ time-of-use pricing.

Current designs of BTES systems rely almost exclusively on the so-called Duct ground heat Storage (DST) model developed some 30 years ago (Hellström, 1989). Engineers design BTES systems according to what the DST model can simulate, and this severely limits the possibility of having original and innovative designs. For example, the DST model only considers an axisymmetric configuration for the boreholes. Furthermore, the number of boreholes in series is the same in all branches, and it is not possible to have simultaneous charging/discharging modes in the BTES.

Steps towards the study of non-axisymmetric BTES geometries have been made by Schulte et al. (2016) with the BASIMO tool and by Cimmino (2018) for series-parallel arrangements. A 3-D transient model of the Drake Landing Solar Community (DLSC) was recently developed (Catolico et al., 2016), but it does not provide the level of detail necessary at the borehole level. Bayer et al. (2014) presented a mathematical procedure for optimization of borehole heat exchanger fields. They showed that it is possible to optimize the load for individual boreholes.

In recent years, high-temperature BTES systems charged with solar heat or industrial waste heat have emerged. A few successful projects such as the DLSC in Canada (Sibbitt et al., 2012) and the industrial waste heat storage system in Sweden (Nordell et al., 2015) have shown that BTES systems have definite potential for such applications.

The design of BTES systems is radically different from regular borehole fields used with ground source heat pump (GSHP) systems. First, boreholes are closely packed, and borehole-to-borehole thermal interaction is much greater and most often beneficial. Secondly, boreholes are typically piped in series while they are piped in parallel in GSHP systems. This creates a radial thermal stratification that reduces heat losses and increases the temperature in the center of the field. A common scheme is to connect boreholes in series and then charge the boreholes from the storage core to the periphery and discharge in the opposite direction whenever needed. In this configuration, simultaneous charging and discharging is not possible unless four-pipe boreholes are used (Marcotte and Bernier, 2019). Another way to have a thermally stratified borehole field is to create two zones with different temperature levels. Each zone can be connected to an independent fluid circuit

fed with its circuit to make simultaneous heating and cooling possible.

Eslami-nejad et al. (2009) have simulated a DT-BTES where solar heat is injected in core boreholes while the temperature of boreholes on the periphery is kept close to the ground temperature to limit unwanted heat diffusion. Panno et al. (2019) used a dual temperature thermal storage configuration, buffer tanks, solar collectors (only for heating), and a heat pump similar to the one considered by Lhendup et al. (2014, 2012) to provide heating for a school building located in Palermo, Italy.

In the present study, a DT-BTES model is proposed. The model is then applied to the geometry presented in Figure 1, consisting of 15 boreholes, each with a length of 183 m. The seven boreholes in the center are connected to a circuit injecting heat in the inner core, and the other eight outer ring boreholes are connected to a heat extracting circuit. As shown in Figure 1, a dual temperature field with core and outer borehole temperatures of ~ 20 and ~ 5 °C, is established.

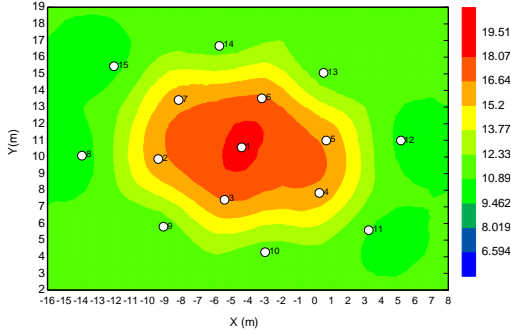


Figure 1: Isotherms for a 15 borehole DT-BTES with heat injection in the center core and heat extraction in the outer boreholes (temperatures are in °C)

In the first part of the paper, the approach used to model borehole heat transfer in such a DT-BTES is presented. Then, the DT-BTES model is used in two simulation test cases. First, a simple case of a heat pump operating between the inner core and the outer ring is presented to show thermal interaction between the two sets of boreholes. Then, an engineering study performed on an actual building (Renovation of the Ontario Association of Architects (OAA) headquarters in Toronto) where a DT-BTES was envisioned is presented. In this case, the objective is to operate heat pumps overnight so that the inner core and the outer ring are hot and cold enough for direct heating and cooling of the building during the daytime.

Methodology

The borehole heat transfer model used in this work has been described by Lecomte and Bernier (2016). This model allows more flexibility than the popular DST model described earlier. For instance, it can consider parallel branches of boreholes connected in series with charge and discharge circuits, and the user determines borehole

positioning. The model calculates the outlet temperature and the heat transfer rate at each borehole in the network and the global outlet temperature and total heat transfer to the ground. It can also evaluate the temperature within the storage between boreholes.

The complete model and the underlying assumptions have been thoroughly presented by Lecomte (2016) and Lecomte and Bernier (2016). Therefore, the modeling approach is only briefly presented here. The DT-BTES geometry of the OAA project will be used to describe the circuitry and borehole interactions. The geometry is presented in Figure 1, where the relative locations of the 15 boreholes are shown; the average distance between two adjacent boreholes is approximately 4.9 meters.

Figure 2.a. shows that the eight outer boreholes and the seven inner boreholes are connected to separate circuits. The outer ring has eight parallel branches, each with one borehole, while the inner ring has seven parallel branches, each with one borehole. Two-pipe (one U-tube) boreholes are used, and the grout used to fill the boreholes is assumed to have the same properties as the ground. Each borehole is subdivided into two sub-boreholes (downward and upward pipes) in series interacting with each other and with the rest of the bore field.

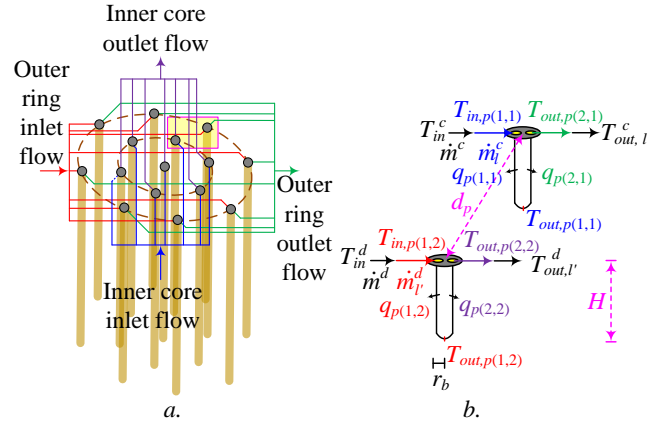


Figure 2: a. Circuit configuration for both groups of boreholes, b. Terminology used for boreholes in each circuit.

Figure 2.b. shows two typical boreholes located on the inner core and outer rings, respectively. Both are connected to their respective circuits (denoted by the superscript “c” for charging and “d” for discharging). The distances r_b , H and d_p represent the borehole radius, the borehole height, and the distance between the two boreholes. The flow rate and inlet temperature of the outer ring and inner core circuits are noted as \dot{m}_c and T_{in}^c and \dot{m}_d and T_{in}^d , respectively. These parameters, as well as borehole dimensions and ground thermal properties, are input parameters to the model. The model determines the outlet fluid temperature of individual

boreholes as well as the global outlet fluid temperature of each circuit (T_{out}^c and T_{out}^d).

For each pipe i in a parallel branch l that includes n_l boreholes connected to circuit “c” (or l' linked to circuit “d”), the following equations can be written:

$$\begin{aligned} T_{in,p(1,l)} &= T_{in}^c \\ \forall i \in (2:2n_l) \quad T_{in,p(i,l)} &= T_{out,p(i-1,l)} \\ T_{out,p(2n_l,l)} &= T_{out,l}^c \end{aligned} \quad (1)$$

Thus, for the two boreholes presented in Figure 2.b $T_{in}^c = T_{in,p(1,l)}$, $T_{out,p(1,l)} = T_{in,p(2,l)}$, and $T_{out,p(2,l)} = T_{out,l}^c$. Similar relations can also be developed for the boreholes on the “d” circuit.

The fluid flow in each branch l or l' can be different from other branches, and the user specifies it as the fraction of the total fluid flow. Therefore, the flow rates of a branch l or l' can be written as $\dot{m}_l^c = FF_l^c \dot{m}^c$ and $\dot{m}_{l'}^d = FF_{l'}^d \dot{m}^d$, where \dot{m}^c and \dot{m}^d are the total flow rates in both circuits and FF_l^c and $FF_{l'}^d$ are the fluid fractions in branches l and l' . Thus, for a BTES with n_{br} branches in the “c” circuit, $\sum_{i=1}^{n_{br}} \dot{m}_i^c = \dot{m}^c$ or similarly $\sum_{i=1}^{n_{br}} \dot{m}_{i'}^d = \dot{m}^d$ for the “d” circuit. The flow fractions are fixed during a simulation, but the total flow rates in both circuits are time-dependent.

As shown in equation 1, the branches are connected in parallel and have the same inlet temperatures for the “c” and “d” circuits (T_{in}^c, T_{in}^d). However, the outlet temperatures ($T_{out,l}^c, T_{out,l'}^d$) differ from one branch to another as they depend on the flow rate, heat transfer rate, and borehole configuration. Finally, the overall outlet temperature of each circuit is calculated by $T_{out}^c = \sum_{i=1}^{n_{br}} FF_l^c T_{out,l}^c$ and $T_{out}^d = \sum_{i=1}^{n_{br}} FF_{l'}^d T_{out,l'}^d$.

The downward and upward pipes in the borehole are assumed to represent sub-boreholes with wall temperature $T_{b,p(i,l)}$ and borehole thermal resistance $R_{b,l}$. This last value is equal to $R_{f,l} + R_{p,l}$, where $R_{f,l}$ and $R_{p,l}$ are the convective and conductive (pipe wall) thermal resistances, respectively.

Using the positions of n_b boreholes provided by the user, the model evaluates the positions of the two pipes in the boreholes. The pipe positions are then used to determine a square matrix, d , of size $2n_b$. This matrix provides the radial distance between two pipes in the BTES. The diagonal components of this matrix, $d_{i,i}$, are equal to the external radius of the pipes $r_{p,o}$ and the non-diagonal components, $d_{i,j}$, represents the center-to-center distance between pipes i and j .

An energy balance for each pipe i located in circuit l , leads to Equations 2.a to 2.d.

$$q_i = \frac{\dot{m}_i^c C_{p,f}}{H} (T_{in,i} - T_{out,i}) \quad (2.a)$$

$$T_{f,i} = \frac{T_{in,i} + T_{out,i}}{2} = T_{b,i} + q_i R_{b,i} \quad (2.b)$$

$$T_{b,i} = T_g + \Delta T_i^* + \sum_{j=1}^{4n_b} q_j h(\Delta t, d_{i,j}) \quad (2.c)$$

$$\Delta T_i^* = \sum_{j=1}^{4n_b} \sum_{k=1}^{m-1} q_j'(t_k) h(t_m - t_{k-1}, d_{i,j}) - q_j(t_{m-1}) h(\Delta t, d_{i,j}) \quad (2.d)$$

where $T_{f,i}$ is the average fluid temperature in pipe i , q_i is the heat transfer rate, $T_{b,i}$ is the pipe wall temperature, $C_{p,f}$ is the fluid heat capacity, T_g is the undisturbed ground temperature, $h(\Delta t, d_{i,j})$ is the thermal response solution which is a function of time, Δt , and radial distance $d_{i,j}$, ΔT_i^* is the aggregated thermal history effect of the previous $m - 1$ time steps of all pipes towards pipe i , $q_j'(t_k) = q_j(t_k) - q_j(t_{k-1})$.

The set of equations 2.a. to 2.d. has a total of $4n_b$ unknowns: for each borehole, there are $2n_b$ pipe outlet temperatures, $T_{out,i}$, and $2n_b$ pipe heat transfer rates, q_i . These unknowns can be determined by solving the equations for given values of T_{in}^c , T_{in}^d , \dot{m}^c , \dot{m}^d , and borehole characteristics. The equations can be reformatted and presented in a simplified matrix format, $AX = B$ (Lecomte and Bernier, 2016). A is a square matrix for the coefficients, and matrix B gives the known results. The solution at time t_m can be obtained using matrix inversion.

For the two boreholes presented in Figure 2.b, the equations in the matrix format are as follows:

$$A = \begin{pmatrix} a_l^c & 0 & 0 & 0 & 1 & 0 & 0 & 0 \\ -a_l^c & a_l^c & 0 & 0 & 0 & 1 & 0 & 0 \\ 0 & 0 & a_{l'}^d & -a_{l'}^d & 0 & 0 & 1 & 0 \\ 0 & 0 & 0 & 0 & a_{l'}^d & 0 & 0 & 1 \\ -1/2 & 0 & 0 & 0 & h_{1,1} + R_{b,l} & h_{1,2} & h_{1,3} & h_{1,4} \\ -1/2 & -1/2 & 0 & 0 & h_{2,1} & h_{2,2} + R_{b,l} & h_{2,3} & h_{2,4} \\ 0 & 0 & -1/2 & -1/2 & h_{3,1} & h_{3,2} & h_{3,3} + R_{b,l'} & h_{3,4} \\ 0 & 0 & 0 & -1/2 & h_{4,1} & h_{4,2} & h_{4,3} & h_{4,4} + R_{b,l'} \end{pmatrix}_{8 \times 8} \quad (3.a)$$

$$X^{-1} = (T_{out,1} \quad T_{out,2} \quad T_{out,2'} \quad T_{out,1'} \quad q_{1,1} \quad q_{2,1} \quad q_{2,1'} \quad q_{1,1'})_{1 \times 8} \quad (3.b)$$

$$B^{-1} = (a_l^c T_{in}^c \quad 0 \quad 0 \quad a_{l'}^d T_{in}^d \quad \frac{T_{in}^c}{2} - T_g - \Delta T_{1,l} \quad -T_g - \Delta T_{2,l} \quad -T_g - \Delta T_{2,l'} \quad \frac{T_{in}^d}{2} - T_g - \Delta T_{1,l'})_{1 \times 8} \quad (3.c)$$

where $a_l^c = \frac{\dot{m}_l^c C_{p,f}}{H}$, $a_{l'}^d = \frac{\dot{m}_{l'}^d C_{p,f}}{H}$. With X , the outlet temperature of the “c” and “d” circuits can be determined as

$T_{out}^c = \sum_{i=1}^{n_{br}} FF_l^c T_{out,l}^c$ and $T_{out}^d = \sum_{i=1}^{n_{br}} FF_{l'}^d T_{out,l'}^d$, where the outlet of each branch (i.e., each borehole) l (or l') can be evaluated as $T_{out,l}^c = T_{out,p(2n_l,l)}$ and $T_{out,l'}^d = T_{out,p(1,l')}$.

The thermal responses, $h(\Delta t, d_{i,j})$ are evaluated here using the so-called Finite Linear Source (FLS) analytical solution. The FLS accounts for radial and axial heat transfer around boreholes. This solution is calculated here by assuming that the borehole is composed of one segment. Thus, the temperature issued from the model can be considered to be the average temperature over the borehole height. Equation 3 reflects the use of spatial and temporal superposition to account for borehole-to-borehole heat transfer and the evolution of borehole heat transfer with time. The thermal response factors are pre-calculated before the first time step for a limited number of time steps (~ 70) to limit calculation

time. During simulations, response factors and then approximated numerically using a cubic spline type interpolation. Lecomte and Bernier (2016) reported that the model was successfully verified against the model developed by Chapuis (2009).

Applications

The model presented in the previous section has been coded into a TRNSYS Type (Type 263) and is used alongside other established TRNSYS models in two application cases. In the first case, a heat pump is used to charge the inner core using heat extracted from the outer ring. In the second application, a DT-BTES system proposed to heat and cool a commercial building is discussed. Both applications use the 15 borehole oval geometry presented in Figure 1. The ground and borehole characteristics are given in Table 1. The fluid is assumed to have properties similar to water.

Table 1: Characteristics of the boreholes

Parameter	Value	units
Ground temperature, T_g	10	°C
Ground and grout thermal conductivity, k_g	1.75	W/m-K
Ground thermal capacitance, $\rho C_{p,g}$	1842	kJ/m ³ -K
Pipe thermal conductivity, k_p	0.4	W/m-K
Outer pipe radius, $r_{p,o}$	0.016	m
Inner pipe radius, $r_{p,i}$	0.013	m
Center-to-center pipe spacing in boreholes	0.0375	m

Simple charging

Figure 3 shows a schematic representation of this simple charging application. As shown in this figure, two independent fluid circuits link the heat pump's evaporator side to the outer ring and the condenser side to the inner core. Thus, the heat pump extracts heat from the outer ring, thereby reducing the ground temperature in the vicinity of these boreholes. This extracted heat and the added compressor power are then injected into the inner core, increasing the ground temperature in the center.

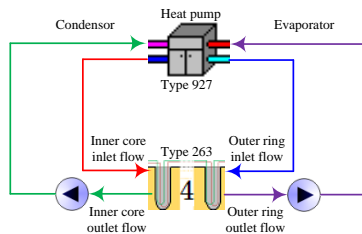


Figure 3: Schematic representation of the simple charging case

The specific conditions of this charging case are presented in Table 2. The heat pump is set to operate 6 hours per day

to examine how ground temperature recovers. The water-to-water heat pump model of TRNSYS (Type 927) is used with its default performance map.

Table 2: Specific input conditions for both cases

Parameter	Simple charging	OAA building	units
Outer ring total flow rate, \dot{m}^c	14400	17280	kg/h
Inner core total flow rate, \dot{m}^d	14400	17280	
Borehole depth, H	183	183	m
Solar collector area	-	140	m ²
Heat pump capacity	24	40	Tons
Heating and cooling COP at rating conditions	5.0	5.0	-
Heat pump performance	Default values of Type 927	Default values of Type 927	-
Heat pump operation	Midnight to 6 am	See control sequence in Table 3	-

Isotherms in the bore field after one year of operation have been shown earlier in Figure 1. A close-up view of the isotherms near an outer borehole (#15) is presented in Figure 4 at two different times: at 6 am of the last day of the first year (heat pump was ON for the previous 6 hours) and 18 hours later (heat pump was OFF during that period). From these two figures, it can be seen that the inner core is at ≈ 20 °C and the periphery boreholes are at ≈ 5 °C after one year of operation (Figure 1). It can also be seen that the size of the cold region near the outer ring boreholes caused by heat extraction has diminished after 18 hours of inactivity. This thermal recovery is caused by heat conduction from the neighboring ground (at 10 °C) and the warm inner core.

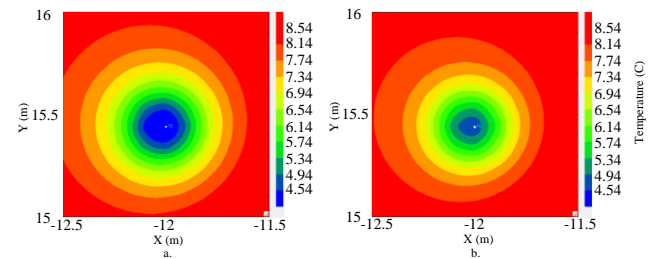


Figure 4: Isotherms around the 15th borehole at 6 am on the last day (a) of the first year and 18 hours later (b)

Figure 5 shows the outlet temperature from the inner core and outer ring over a five-year period. Both curves exhibit a band of temperatures of the order of 5 °C, indicative of the daily temperature variations caused by intermittent heat pump operation. The outlet temperature from the inner core increases from an initial value of 10 °C up to ≈ 25 °C at the

end of the fifth year. The outlet temperature from the outer ring decreases during the first month due to heat extraction from the heat pump. Then, the outlet temperature increases gradually over time. This increase is caused by heat conducted from the core which is greater than the one extracted by the heat pump in the outer ring boreholes. This seems to indicate that some of the heat losses from the core are picked up by the outer boreholes.

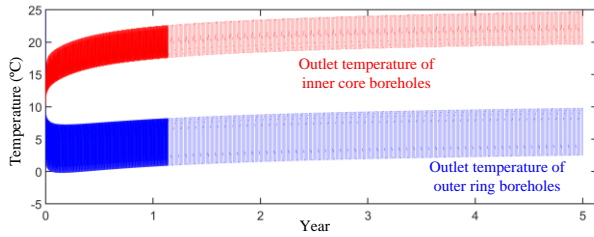


Figure 5: Outlet temperatures over five years for the simple charging test

Investigation of the DT-BTES concept for an actual building

The DT-BTES concept was examined at the design phase for the Ontario Association of Architects (OAA) headquarters in Toronto. The DT-BTES geometry used thus far in this article and shown in Figure 1 has been suggested to provide heating and cooling of the OAA building. The geometry was fixed by the designer and borehole drilling had been initiated when the present authors got involved in the project. One of the objectives was to determine if it would be possible to heat and cool this building with a DT-BTES without operating the heat pump during the daytime when the electricity is more likely to have a high CO₂/kWh content.

The heating and cooling system configuration is presented in Figure 6 using the TRNSYS simulation studio window format. The maximum hourly heating and cooling loads of this building are 110 and 112 kW, respectively. A 40-ton heat pump meets these loads.

The heating and cooling loads (red and dark blue circuits in Figure 6) are met using hot and cold water from two buffer tanks. These 100 m³ tanks are connected to the evaporator and condenser sides of the heat pump. The design setpoint temperatures of these tanks are 40 and 8 °C, respectively. On the evaporator side (green circuit in Figure 6), the fluid at the heat pump's exit feeds the cold tank first and then goes to the outer ring boreholes. On the condenser side (orange circuit in Figure 6), the fluid at the heat pump's exit feeds the hot tank first and then goes to the inner core boreholes. For certain cases (see discharge mode in Table 3), the evaporator side of the heat pump is connected to the inner core to take advantage of a high source temperature when hot tank heating is required. In this case, the pink and light blue circuits are active. Also, solar collectors are used to add heat to the inner core. Thus, when solar energy is available,

a portion of the main flow (orange circuit) is bypassed to go through solar collectors.

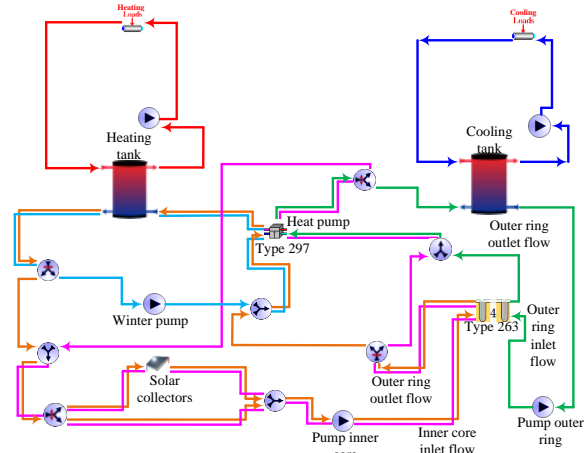


Figure 6: TRNSYS assembly and possible circuits for the OAA DT-BTES concept

The solar collector efficiency is evaluated using the standard TRNSYS solar collector model, which essentially evaluates the solar collector efficiency using the following equation:

$$\eta = 0.7 - 15(T_{in, coll.} - T_{amb.})/G_t \quad (4)$$

where $T_{in, coll.}$ is the inlet temperature to the collector (°C), $T_{amb.}$ is the ambient temperature (°C) and G_t is the total incident solar radiation (kJ/kr-m²). This equation leads to a 70% efficiency when $T_{in, coll.}$ is equal to $T_{amb.}$

The control sequence for this case is presented in Table 3, and characteristics of the various components are given in Table 2.

The **Charge-mode** operates at night for only 3 hours, from 9 pm to 12 am. In this mode, the heat pump functions continuously, cooling the outer ring and heating the inner core.

The **Discharge-mode** is used overnight to charge the hot water tank for space heating of the building during the day. This mode operates from 12 am to 8 am in the winter months and from 12 am to 5 am in the other months. This is accomplished in two stages. First, fluid is pumped from the inner core (via the orange circuit) to heat the tank directly; the heat pump is inactive. In the second stage, the heat pump is active, and the evaporator side is connected to the inner core (pink circuit), and the condenser side supplies hot water to the tank (light blue circuit). This takes advantage of relatively high supply temperatures to the heat pump, which increases its performance. Note that the discharge mode is deactivated when the setpoint temperature is reached.

In **Inactive-mode**, the heat pump is inactive between 5 am (or 8 am), and 9 pm and only gets activated if the cold tank temperature goes above its set point temperature of 8 °C, in which case the cooling-mode is activated (green and orange circuits).

The **solar charging-mode** gets activated when solar availability is high enough (i.e., above 400 kJ/hr-m²). In this mode, part of the main flow is bypassed to the solar collectors.

Table 3: Control sequence used in the simulation for the OAA building

Mode	Details
- Charge mode Heat pump transfers heat from the outer to the inner rings	9 pm to 12 am (3 hours) Green and orange circuits are active. Heat pump is ON
- Discharge mode (Heating only): Charging of the hot tank in 2 stages to its setpoint temperature.	12 to x am Nov. to Feb. x=8am Other months. x=5am - 1st stage : Orange circuit is active. Heat pump is OFF. - 2nd stage: Pink and light blue circuits are active. Heat pump is ON.
- Inactive mode: The heat pump is inactive unless the cold tank requires cooling (see cooling mode).	from 5 am (or 8 am) until 9 pm
- Cooling mode: Cooling mode overrides the inactive mode when the cold tank requires cooling (temperature is above 8 °C).	Green and orange circuits are active. Heat pump is ON
- Solar charging mode: When solar availability is high enough (i.e., above 400 kJ/hr-m ²)	Part of the flow in the orange or pink circuits is bypassed to the solar collectors

The system was simulated for five years with a one-hour time step. Figure 7 shows the resulting average monthly heat pump energy consumption in Year 5 for each hour of the day (Y5-M1 represents the first month of year 5). Results show that the energy consumption is relatively high (at around 110 000 kJ) for every month when the heat pump is turned ON at 9 pm. The energy consumption stays high for the winter months until the following day, indicating that the heat pump is still ON. For summer months (June to September), the heat pump is essentially OFF starting at 2 am. The striking feature of Figure 7 is that the heat pump energy consumption is virtually zero between 9 am to 9 pm except for a small blimp for July and August at around 18h. Thus, it appears that it is possible to heat and cool this building with a DT-BTES without operating the heat pump during the daytime.

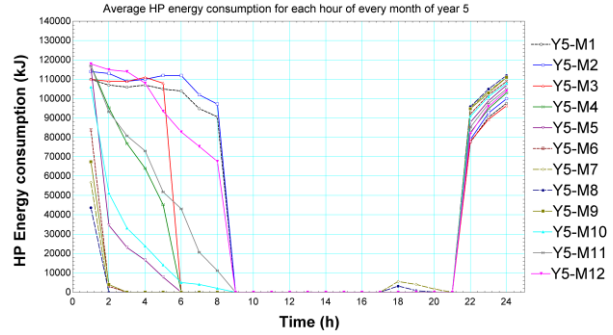


Figure 7: Average heat pump energy consumption for each hour of every month for Year 5

As shown in Figure 8, the temperature of the outer ring boreholes during the summer is cold enough to provide “free” cooling to the cold tank, and the inner core remains in the 15 to 25 °C temperature range throughout the year. This temperature is high enough for efficient heat pump operation and low enough to limit heat losses from the BTES.

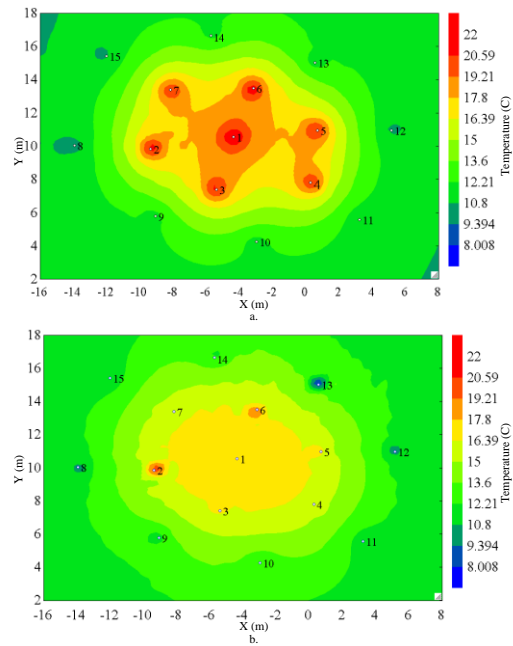


Figure 8: Isotherms at the end of July and December for year 5

Figure 9.a shows the outlet temperature of the inner core and outer ring during the five year period. It can be seen that the outlet temperature of the inner core shows essentially the same pattern from year to year. On the other hand, the outlet temperature of the outer ring increases ~2°C during this period, which indicates that inner core conduction towards the outer ring increases over time.

Figure 9.b shows that the outlet temperature from both tanks that provide heating and cooling of the building. Both

temperatures have some transient variations in the first year of operation. After that initial period, the hot and cold tank temperature profiles are in quasi-steady-state. The outlet temperature of the heating tank goes down to about 25 °C in the winter and stays in the 35-40 °C range for the rest of the year. The outlet of the cold tank rarely goes above 10 °C.

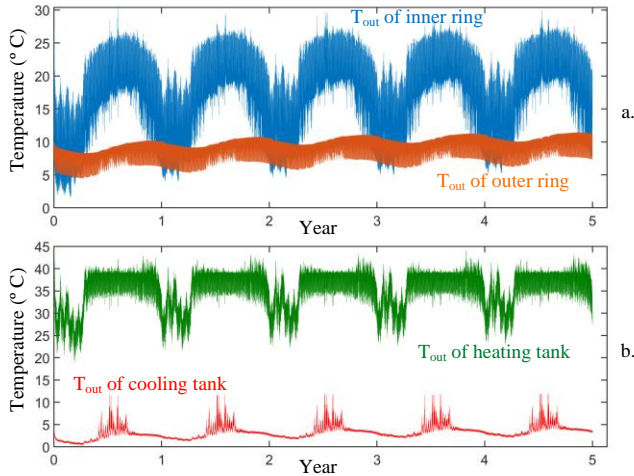


Figure 9: Outlet temperatures from the two circuits and the two tanks over a 5 year period

Columns 2 to 5 in Table 4 present the annual heat pump energy consumption, $HP_{cons.}$, injected solar heat, $S_{inj.}$, solar collector efficiency, η , and combined COP, for the OAA case. The combined COP is defined as the sum of the annual heating (4.25E8 kJ) and cooling loads (9.85E7 kJ) over the annual energy consumption of the heat pump. The last two columns show results obtained when the 15 boreholes are used in a traditional geothermal heat pump operation (Bernier, 2018). In this case, the heat pump is allowed to operate normally to meet the building load at any given hour of the day, and there are no solar collectors.

Results in Table 4 show that the proposed control sequence operation leads to relatively low COP values. For example, in year five, the COP is 2.13. This low value can be explained by the fact that a relatively large amount of energy is stored in the ground and not accounted for in the definition of the COP. This variation of the internal energy of the DT-BTES cannot currently be evaluated by the model presented here. In comparison, the COP of the traditional geothermal heat pump is 4.78 in year 5.

It can also be seen that the solar collector efficiency is relatively high, with a year five average of 60%. This is due to the relatively favorable inlet temperatures to the collectors throughout the year. Finally, Table 4 shows that the DT-BTES performance reaches a quasi-steady-state condition after five years of operation.

Table 4: Results of OAA simulations compared to a regular heat pump operation

Year	With the control sequence of Table 3				Regular HP operation	
	$HP_{cons.}$ (kJ)	$S_{inj.}$ (kJ)	η (-)	COP (-)	$HP_{cons.}$ (kJ)	COP (-)
1	2.50E8	4.63E8	0.63	2.09	1.09E8	4.80
2	2.49E8	4.53E8	0.61	2.10	1.10E8	4.78
3	2.48E8	4.49E8	0.61	2.11	1.10E8	4.77
4	2.47E8	4.46E8	0.60	2.12	1.10E8	4.77
5	2.45E8	4.44E8	0.60	2.13	1.10E8	4.78

Figure 10 gives a snapshot of results obtained during a summer hour. In this case, the system is working in cooling mode with solar charging (see control sequence in Table 3). Water exits the cold tank at 8.2 °C and is fed to the cooling coil. It returns to the cold tank at 13.2 °C. The evaporator side of the heat pump is fed with 17280 kg/h of 10.1 °C water from the outlet of the outer boreholes. Water is cooled down to 6.8 °C in the heat pump and fed to the cold tank. On the condenser side, water exits the heat pump at 37.7 °C and is sent to the hot tank to recharge it. Water exits in the hot water tank at 34.7 °C. Then, about half of the total flow rate is directed to solar collectors. Water exits the solar collectors at 40 °C and is mixed with the main flow to enter the bore field's inner core at 37.9 °C. Finally, energy is transferred into the inner core boreholes, and the fluid exits at 32.6 °C and is fed to the condenser inlet.

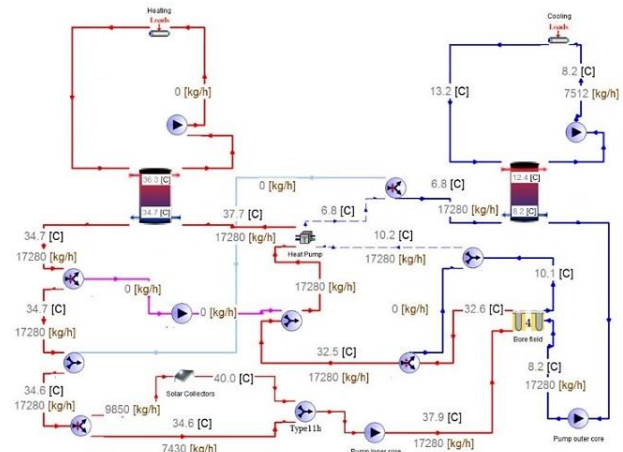


Figure 10: Typical results when the cooling and solar charging modes are active

Conclusion

The dual temperature Borehole Thermal Energy Storage (DT-BTES) system presented in this paper consists of warm boreholes in an inner core surrounded by colder boreholes on an outer ring. The dual temperature can be created using

a heat pump that extracts heat from the outer boreholes and injects it back to the inner core.

In the first part of this paper, the borehole modeling strategy for the DT-BTES system is presented. The proposed model can handle parallel branches of boreholes connected in series and accounts for borehole thermal interaction. It is also possible to have simultaneous charging and discharging circuits, a definite advantage over the popular DST model. Borehole heat transfer is calculated using the Finite Line Source analytical solution.

The model is then used to simulate the operation of a DT-BTES that consists of 15 boreholes in two different test cases. The first test shows that the outlet temperature of the outer ring rises after a few months of operation even though heat is extracted from these boreholes. This is due to heat conduction from the inner core, which reaches the outer boreholes after a certain period.

In the second test case, it is shown that it is possible to deactivate the heat pump during the daytime hours (9 am to 9 pm) and rely on stored energy to provide direct heating and cooling of a building during the daytime. This mode of operation leads to a relatively low COP value of 2.13. However, since the heat pump operates overnight to charge the DT-BTES, it can use electricity with lower CO₂ content.

References

- Bayer, P., M. de Paly, and M. Beck. 2014. Strategic optimization of borehole heat exchanger field for seasonal geothermal heating and cooling, *Applied Energy*, 136:445-453.
- Bernier, M., 2018, Modeling and simulation of the inner-outer loop concept for the OAA headquarters, confidential final report prepared for WSP, 53 pages.
- Catolico, N., S. Ge, and J.S. McCartney. 2016. Numerical modeling of a soil-borehole thermal energy storage system, *Vadose Zone Journal*, February 2016. 1-17.
- Chapuis, S., 2009. Stockage thermique saisonnier dans un champ de puits géothermiques verticaux en boucle fermée, Montréal, Québec, Canada: Mémoire de maîtrise, École Polytechnique de Montréal.
- Chapuis, S., Bernier, M. 2009. Seasonal storage of solar energy in boreholes, *Proceedings of the 11th International IBPSA conference*, 27-30 July, Glasgow, Scotland, 599-606.
- Chapuis, S., Bernier, M. 2008. Étude préliminaire sur le stockage solaire saisonnier par puits géothermiques, 3rd Canadian Solar Buildings Conference, Frédéricton, Nouveau-Brunswick, 14-23.
- Cimmino, M. 2018. A finite line source simulation model for geothermal systems with series-and parallel-connected boreholes and independent fluid loops, *J. of Building Performance Sim.*, 11(4), 414-432.
- Eslami-nejad, P., A. Langlois, S. Chapuis, M. Bernier and W. Faraj. 2009. Solar heat injection into boreholes, *Proceedings of the 4th Canadian Solar Buildings Conference*, 25-27 June, Toronto, 237-246.
- Gehlin, S. 2016. Borehole thermal energy storage (Chapter 11). In: Simon J. Rees, editor. *Advances in ground-source heat pump systems*. Woodhead Publishing; 63-95.
- Hellström, G. 1989. DST Duct ground storage model, *Manual for Computer Code*.
- Lecomte, C. 2016. Modélisation de champs de puits géothermiques en série pour un stockage thermique saisonnier, *Mémoire de maîtrise*, École Polytechnique de Montréal.
- Lecomte, C. and M. Bernier. 2016. Modélisation et simulation de puits géothermiques en série pour stockage saisonnier. *Proceedings of the eSim 2016 Conference*, May 3-6, McMaster University, Hamilton, Ontario, Canada, pp. 265-276.
- Lhendup, T., Aye, L., and R.J. Fuller 2014. Thermal charging of boreholes. *Renewable energy*, 67, 165-172.
- Lhendup, T., Aye, L., and R.J. Fuller. 2012. Experimental study of coolth charging of an inter-seasonal underground thermal storage system. 50th annual AuSES conference. Swinburne University of Technology, Hawthorn Campus Melbourne, Australia.
- Marcotte, B. and M. Bernier. 2019. Experimental validation of a TRC model for a double U-tube borehole with two independent circuits, *Applied Thermal Engineering*, 162:114229.
- Nordell, B., Andersson, O., Rydell, L., and A. Liuzzo-Scorpo. 2015. Long-term performance of the HT-BTES in Emmaboda, Sweden. In: *Proc. Greenstock 2015*, Beijing, China, 1-8.
- Panno, D., Buscemi, A., Beccali, M., Chiaruzzi, C., Cipriani, G., Ciulla, G., ... and Bonomolo, M. 2019. A solar assisted seasonal borehole thermal energy system for a non-residential building in the Mediterranean area. *Solar Energy*, 192, 120-132.
- Schulte, D.O., W. Rühaak, B. Welsh, and I. Sass. 2016. BASIMO – borehole heat exchanger array simulation and optimization tool. *Energy Procedia*, 97, 210-217.
- Sibbit, B, D. McClenahan, R. Djebbar, J. Thornton, B. Wong, J. Carriere, and J. Kokko. 2012. The performance of high solar fraction seasonal storage district heating system – five years of operation. *Energy Procedia* 30:856-865.
- Teamah, H. M., and M.F. Lightstone 2019. Numerical study of the electrical load shift capability of a ground source heat pump system with phase change thermal storage. *Energy and Buildings*, 199, 235-246.